Logic Operations Based on Magnetic-Vortex-State Networks

Hyunsung Jung,[†] Youn-Seok Choi,[†] Ki-Suk Lee,[†] Dong-Soo Han,[†] Young-Sang Yu,[†] Mi-Young Im,[‡] Peter Fischer,[‡] and Sang-Koog Kim[†],*

[†]National Creative Research Initiative Center for Spin Dynamics and Spin-Wave Devices, Nanospinics Laboratory, and Research Institute of Advanced Materials, Department of Materials Science and Engineering, College of Engineering, Seoul National University, Seoul 151-744, Republic of Korea and [‡]Center for X-ray Optics, Lawrence Berkeley National Laboratory, Berkeley, California 94720, United States

I n current semiconductor technology, the electron charge is the basic operational unit in information-processing devices. The major limitation of that technology in cases of nanoscale electron channels is the significant electron leakage and inevitable energy loss.[1,2] This demands additional research into new practical alternatives. One such alternative is to use switchable magnetization states. For example, some earlier works[3−5] report magnetic quantum dot cellular automata that consist of single-domain magnets. Possible logic operations using closed-flux states in ring-type magnets have also been reported.[6−8] Barman *et al.* proposed a new type of signal transfer mechanism based on vortex-state disk chains and coupled gyrations, as studied by micromagnetic simulations.[9] These alternatives promise to significantly reduce the energy dissipation and avoid the electron leakage problem.

Here, we propose an additional solution— logic operations based on magnetic-vortex-state networks—and report an experimental demonstration of a simple, archetypal XOR logic operation achieved *via* a robust vortex-gyration-mediated information-signal transfer mechanism.[9−14] The advantages are unlimited signal transfer endurance, low-energy dissipation, and low-power signal inputs *via* resonant vortex excitation. This work paves the way for a new type of logic operation based on magnetic-vortex-state networks.

It is known that magnetic-vortex gyration in a confined potential is the low-frequency eigenmode of the translational orbital motion of a single vortex core, around its equilibrium position, at a characteristic eigenfrequency, ω_D.[15] If the frequency, ω_H, of any driving force is tuned to ω_D, the vortex gyration can readily be excited resonantly, even with extremely low power consumption,

ABSTRACT
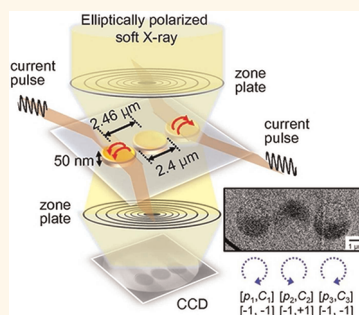
Logic operations based on coupled magnetic vortices were experimentally demonstrated. We utilized a simple chain structure consisting of three physically separated but dipolar-coupled vortex-state Permalloy disks as well as two electrodes for application of the logical inputs. We directly monitored the vortex gyrations in the middle disk, as the logical output, by time-resolved full-field soft X-ray microscopy measurements. By manipulating the relative polarization configurations of both end disks, two different logic operations are programmable: the XOR operation for the parallel polarization and the OR operation for the antiparallel polarization. This work paves the way for new-type programmable logic gates based on the coupled vortex-gyration dynamics achievable in vortex-state networks. The advantages are as follows: a low-power input signal by means of resonant vortex excitation, low-energy dissipation during signal transportation by selection of low-damping materials, and a simple patterned-array structure.

as already demonstrated in earlier works.[16−19] The gyration's rotational sense is determined by the vortex-core orientation, that is, counterclockwise for the up core (polarization, $p = +1$) and clockwise for the down core ($p = -1$).[15] When isolated vortex-state thin-film disks are sufficiently close to each other, the vortex gyrations of the neighboring individual disks are coupled *via* their respective dynamically rotating stray fields,[11−13] which coupling provides the opportunity for mutual energy transfer and frequency

Disk 1
$[p_1, C_1]$
$[-1, -1]$

Disk 2
$[p_2, C_2]$
$[-1, +1]$

Disk 3
$[p_3, C_3]$
$[-1, -1]$
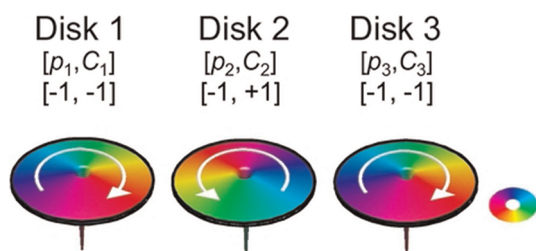
Figure 1. Coupled magnetic-vortex-state network. Model geometry of three Permalloy (Py) disks of indicated initial ground states. The local in-plane magnetizations inside each disk are represented by the colors shown in the color wheel (inset), and the curling orientations are indicated by the white arrows (chirality, $C = +1$ and -1 for CCW and CW rotational sense, respectively). The spike at the center of each disk indicates the out-of-plane component of the core magnetization (polarization, $p = +1$ and -1 for the up core and down core, respectively). For micromagnetic numerical simulations, equal diameter $2R = 300$ nm, thickness $L = 6.0$ nm, and center-to-center distance $d_{int} = 330$ nm were used.

splitting, as found in a variety of coupled oscillators existing in nature.[20]

RESULTS AND DISCUSSION

Design of Archetypal XOR Logic Gate by Simulations. On the basis of our recently demonstrated robust mechanism of vortex-gyration-mediated energy and consequent information-signal transfer between neighboring vortex-state disks, the next milestone toward the realization of vortex-state-network-based logic gates, for example, using three vortex-state Permalloy (Py) disks, is presented here. If two electrodes are positioned on both Py end disks (hereafter, disk 1 and disk 3), the "1" logic function input state can be initiated by applying currents to either or both electrodes and exciting, thereby, vortex gyrations. The gyration of the center disk (hereafter, disk 2), which is stimulated by the gyrations of either disk 1 or disk 3, can be represented as the "1" logical output and can be monitored. To study our concept, we first conducted micromagnetic simulations of magnetic-vortex-state networks comprising three different Py disks (see Figure 1). Figure 2 illustrates the trajectories of vortex-core gyrations in the individual disks for three different logical inputs: the application of currents to both disks 1 and 3, representing the "11" logical input, yields the excitation of large-amplitude vortex gyrations in disks 1 and 3. For the specific case of $p_1p_3 = +1$ (where the numbers in subscripts indicate the disks), the "11" logical input yields the "0" logical output since the vortex excitation of disk 2 is suppressed. For the cases of applications of currents to either disk 1 or disk 3, which is referred to as the "10" or "01" logical state, by contrast, these inputs give rise to the "1" logical output, as represented by the sufficiently large gyration amplitude in disk 2. The gyration in disk 2 is stimulated by the gyration of disk 1 or 3 *via* the dipolar interaction

between the nearest neighboring disks as reported in ref 11. These logical functions represent an XOR gate.

In order to elucidate such contrasting behaviors between the "11" and "10" logic inputs, that is, suppressed excitation *versus* large-amplitude-gyration excitation in disk 2, we considered the vector sum of the dynamically rotating stray fields produced by the non-zero net in-plane magnetizations of both end disks (see Figure 2, right panel). When the cores are shifted from their initial center positions and gyrate at their own ω_D, the stray fields also rotate at the same frequency as ω_D but with a certain ellipticity, which is defined as the ratio of the field strength along the x-axis to that along the y-axis. Therefore, these fields can be referred to as "elliptically rotating dynamic fields". Here, for the case of parallel polarizations in the end disks ($p_1p_3 = +1$), the net resulting stray field inside disk 2 is almost zero for the "11" input, as shown in Figure 2 (left, top). Contrastingly, for the case of "10" or "01", the vortex gyration with the clockwise (CW) rotational sense in either disk 1 or disk 3 results in a counterclockwise (CCW) elliptically rotating field. As reported earlier,[18,21,22] the application of CW rotating fields of $\omega_H = \omega_D$ leads to large-amplitude resonant excitations for the down core but no excitations for the up core, whereas the application of CCW rotating fields produces the opposite effect. The CCW elliptically rotating field applied to disk 2, which results from the vector sum of the CCW and CW circular-rotational fields with a CCW-to-CW amplitude ratio of 2.5, was obtained from a fit to the simulation data. Although the CCW component is 2.5 times larger than that of the CW, this CW component can still excite the gyration of the down core, as evidenced by the trajectory of the core in disk 2 (see Figure 2, left, bottom). If the core were upward, the gyration amplitude would have been larger than was measured in the present case.

Experimental Verification Using Soft X-ray Microscopy. Next, the XOR gate concept was experimentally confirmed through vortex gyration propagation in an array of vortex-state disks. The vortex-state network consisted of three physically separated but dipolar-coupled Py disks and, for application of logical inputs, two electrodes on each disk. Specifically, for the "1" logical input, external driving forces in the form of magnetic fields (or spin-polarized currents) were applied to disk 1 and/or disk 3, and as the "1" logical output, vortex gyrations excited in disk 2 was utilized. We directly measured, as logic output state, the dynamic excitations of the vortex gyrations in disk 2, while simultaneously monitoring those in disks 1 and 3 using the large field of view offered by the time-resolved full-field soft X-ray microscopy (see Figure 3) (temporal resolution = 70 ps; spatial resolution = 25 nm; see Materials and Methods),[13,24] and employing X-ray magnetic circular dichroism (XMCD) as magnetic contrast. The respective initial ground states of the
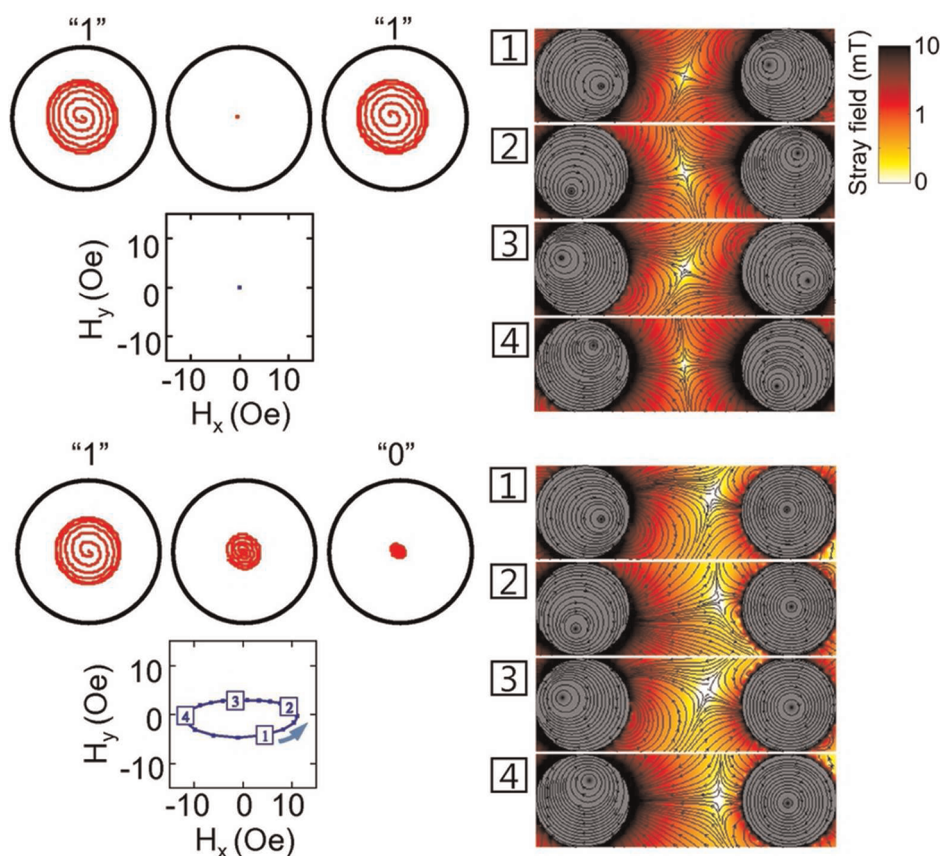
Figure 2. Simulation results for coupled vortex gyrations. Trajectories of vortex-core gyrations in three disks of initial vortex states indicated in Figure 1 for two logical inputs "11" and "10" (left top and bottom, respectively). As described in the text, the logical input "1" indicates the presence of resonant vortex gyration excited by the application of input currents. The spatial distributions of the effective local rotating fields in disk 2, which are the results for the sum of the stray fields generated by the shifted core motions of disk 1 and/or disk 3 (right panel). The local fields averaged inside the disk 2 over one cycle gyration are given just below the corresponding disk 2 (left panel), along with the rotational sense of the field indicated by the corresponding arrow.

disks in the real sample are shown in the inset of Figure 3. The chirality of each disk was determined directly by the in-plane magnetization contrast, whereas the polarization was derived from the rotational sense of the vortex gyrations in the three disks, as indicated. Note that we used larger dimensions of samples than those employed in the simulations because of the experimental limitations of detecting gyration signals using soft X-ray microscopy and since the main dynamic behaviors of coupled gyrations and logic functions between smaller- and larger-dimension samples are not much different, except for the eigenfrequency.

To enhance the contrast view of the time-resolved images, differential images (see Figure 4) were obtained by subtracting two different XMCD images of a π phase difference.[25] A series of differential images of π phase difference, provided in Supporting Information Figure S1, show only the dynamic changes of the individual disks' magnetizations during their vortex-core motions. Given the absence of any core gyration, the static magnetization contrast was removed so that there would be no contrast around the core region.

Accordingly, from those differential images, we identified the logical input and output states. For the "10" (top) and "01" (bottom) input states, the logical output is indicated to be the "1" state. The relatively dark and white contrasts in disk 2 evidence the gyration. For the "11" input state, the "0" output state appears, as represented by the no gyration (no any contrast) of disk 2 in the differential image (see Figure 4 and Supporting Information Figure S2). These functions represent the XOR logic. This experimental demonstration provides a promising foundation for the practical realization of logic devices based on vortex-state networks and readily controllable vortex-gyration dynamics.

Programmable Logic Operations. It is interesting to note that for the antiparallel polarization $p_1p_3 = -1$, unlike the "11" input signal result for the $p_1p_3 = +1$ case, vortex gyrations were resonantly excited in disk 2, leading to the "1" logical output (see Supporting Information Figure S3), as found from additional simulations. For the logical input of either "10" or "01", the vortex gyration remained excited in disk 2, which situation is referred to as the "1" logical state. Therefore, for
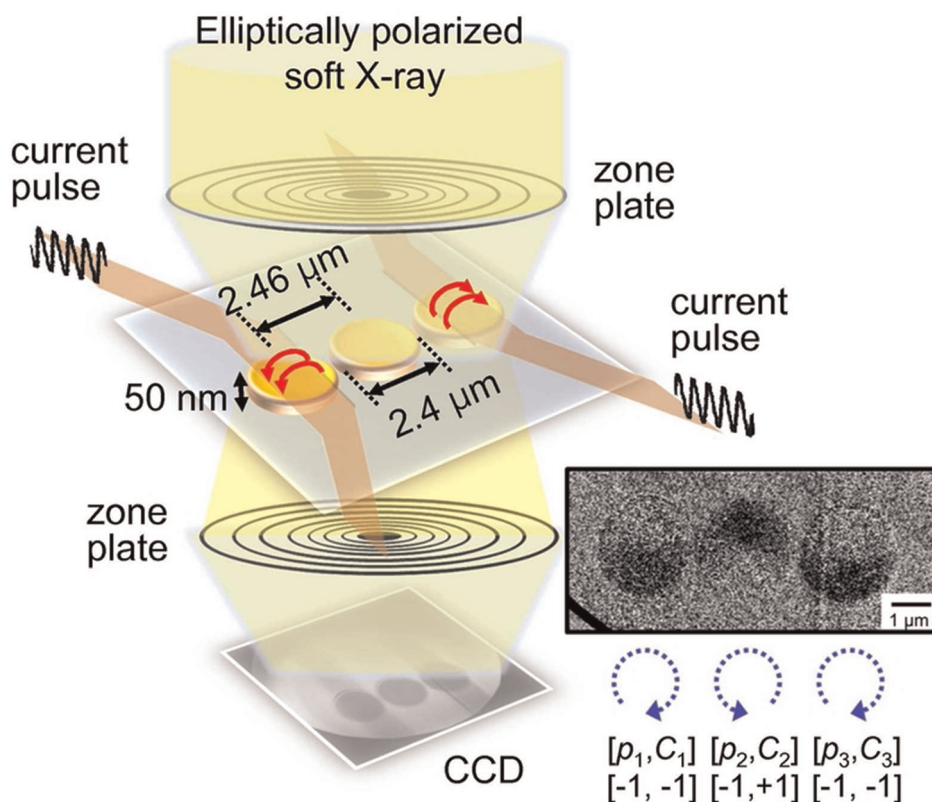
Figure 3. Experimental setup for the direct demonstration of XOR logic operation using the indicated vortex-state network and full-field soft X-ray microscopy. Schematic layout of soft X-ray measurement setup for direct readout of output signals in disk 2, showing the sample (chain of three vortex-state Py disks) with electrodes on both end disks for application of input signals. Equal diameter $2R = 2.4$ μm, thickness $L = 50$ nm, and center-to-center distance $d_{int} = 2.46$ μm are used for the experimental sample. The right inset shows the initial ground vortex states measured by the microscope through XMCD contrast (the same as those shown in Figure 1). Sinusoidal oscillating magnetic fields of 4.5 Oe amplitude and 160 MHz frequency are applied to disk 1 and/or disk 3.
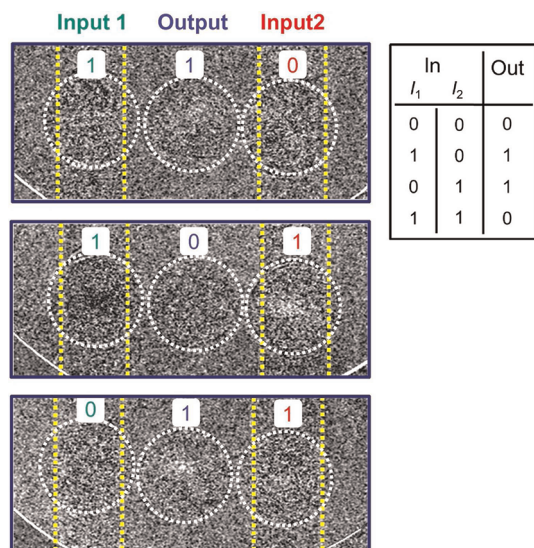

Figure 4. Differential XMCD images of individual disks' vortex gyrations. Three different logical inputs of "10", "11", and "01" are applied. The inset shows the truth table representing the logical input and resultant output operations for the XOR gate.

the $p_1p_3 = -1$ configuration, the employed logic function is an OR gate, as shown in Table 1. The polarization

TABLE 1. Truth Table for Possible Logical Inputs and Resultant Outputs for All Relative Polarization Configurations in a Chain of Three Vortex-State Disks[a]

p_1	1	1	-1	-1	-1	1	1	-1
p_2	1	-1	1	-1	1	1	-1	-1
p_3	1	1	-1	-1	1	-1	-1	1

input		output (disk 2)			
disk 1	disk 3	$p_1p_3 = 1$		$p_1p_3 = -1$	
0	0	0		0	
1	0	1		1	
0	1	1	XOR	1	OR
1	1	0		1	

[a] The resultant logic operation is an XOR gate for $p_1p_3 = +1$ (parallel polarization) or an OR gate for $p_1p_3 = -1$ (antiparallel polarization).

of either disk 1 or disk 3 can be readily reversed by a low-power-consumption oscillating field or pulses, as found earlier.[17−19,22,26] Thus, by manipulating the relative polarization configurations of both end disks with the same electrodes as those for application of logic inputs,

the XOR and OR gates can be programmed; the XOR gate for the equal polarization $p_1p_3 = +1$ and the OR gate for the antiparallel polarization $p_1p_3 = -1$.

On the basis of simulations considering all relative polarization and chirality configurations, we summarize, in Table 1, the logic outputs in disk 2 for the four input cases "10", "01", "11", and "00". In all of these cases, only two logic gates, XOR and OR, were initiated for $p_1p_3 = +1$ and -1, respectively. We note that neither the relative chirality configurations between disks 1 and 3 nor the polarization or chirality of disk 2 affected the overall logic functions. In order to identify either the logical output "0" or "1" in the present work, we monitored, by soft X-ray microscopy, the occurrence of vortex gyrations in disk 2.

We note that the phase control of vortex-gyration excitations as input signals is very essential to the realization of logic devices using coupled vortex gyration propagation. We further conducted numerical calculations using Thiele's equation of motion of magnetizations.[27] From the additional simulation results (see Supporting Information Figure S4), the gyration amplitude in the middle disk (disk 2) varies considerably with the phase difference Δ of the frequencies between two magnetic fields applied to disks 1 and 3. The phase differences of less than 30 degrees nonetheless results in the gyration amplitude of disk 2, which is as small as 25% of those of disks 1 and 3. The fact of the dependence of the gyration amplitude of disk 2 on Δ is rather promising with regard to control of the signal gain of vortex gyration and different logic functions by manipulation of the phase difference of the two input signals.

As for the readout of logical output signals in real devices, vortex gyrations excited in the middle disk can be detected by electrical measurements based on the fact that shifted cores result in asymmetry of in-plane curling magnetizations with respect to the ground vortex state. Therefore, tunneling magnetoresistance in spin-valve structures including vortex-state disks would be markedly variable depending on the amplitude of gyrations excited in the middle disk. For more details of possible detecting mechanisms experimentally demonstrated, see refs 28–30.

Since this work is the first to experimentally demonstrate logic operations using the coupled gyrations of vortex-state disks, several technical issues for the implementations into real devices should be solved in future works; the readout mechanism of vortex excitations and signal-to-noise ratio through electrical measurements of output signals, the threshold value for detection of reliable logical output signals, the asymmetries of the frequency, phase, amplitude of two different input signals, and the delay time and density of integrated logic gates will be clarified.

CONCLUSIONS

Our work demonstrates low energy loss, low-power signal-input logic gates that operate at room temperature on the principle that vortex gyrations are resonantly excited and strongly networked *via* coupling between neighboring vortex-state disks. Notably, the excitation of vortex gyrations and signal transfer between neighboring disks *via* the robust vortex-gyration-mediated mechanism are as fast as a few nanoseconds to a few tens of nanoseconds, depending on the disk dimensions, the separation distance, and the constituent material parameters. Thus, such logic functions can be operated at up to 1 GHz levels by appropriate engineering of materials and disk dimensions. Moreover, by combining different vortex-state networks, a NOR gate can be formed, thereby establishing what is known as universal logic. The advantages are unlimited signal transfer endurance, low-energy dissipation, and low-power signal inputs *via* resonant vortex excitation. All in all, the present work provides a solid foundation for implementation of the static and dynamic properties of coupled magnetic-vortex-state networks into spin-based information processing devices.

MATERIALS AND METHODS

Micromagnetic Simulations. The Landau–Lifshitz–Gilbert (LLG) equation of motion of the local magnetizations was numerically solved on the model system shown in Figure 1, using the OOMMF code.[31] The material parameters of the Py disks of the indicated dimensions were set as follows: exchange stiffness $A_{ex} = 13$ pJ/m; saturation magnetization $M_s = 8.6 \times 10^5$ A/m; magnetic anisotropy constant = 0; gyromagnetic ratio $\gamma = 2.21 \times 10^5$ m/As; damping constant $\alpha = 0.01$. The unit cell size was $3 \times 3 \times 6$ nm³. To resonantly excite vortex gyrations, a continuous sinusoidal oscillating magnetic field of 1 mT amplitude and 210 MHz frequency was applied, 210 MHz being the eigenfrequency of the isolated Py disks.

Sample Preparation. To experimentally demonstrate the proposed logic gate of a coupled vortex-state network, we used three Py disk samples, each of radius $R = 1.2$ μm, thickness $L = 50$ nm, and center-to-center distance $d_{int} = 2.46$ μm, which were deposited onto a 200 nm thick silicon nitride membrane by DC magnetron sputtering. To generate magnetic fields, two electrodes of Ti 10 nm/Cu 100 nm/Au 5 nm were deposited directly on top of both of the end disks by DC sputtering without vacuum breaking. Patterning of the samples was carried out by electron beam lithography and lift-off processing. To avoid adjacent-disk excitations due to the applied local field, the width of the electrodes, as designed, was 1.6 μm.

Soft X-ray Microscopy Measurement. Vortex gyrations in the individual Py disks were directly imaged by full-field magnetic transmission soft X-ray microscopy (MTXM) at beamline 6.1.2 of Advanced Light Source in Berkeley, CA, utilizing a stroboscopic pump-and-probe technique providing 70 ps time and 25 nm spatial resolutions. Details on this time-resolving technique can be found elsewhere.[10,23,24] In-plane magnetization contrast was obtained by monitoring the spatial distribution of the local magnetizations through XMCD at the Fe L_3 absorption edge, where the sample surface was positioned at a 60° orientation to

the propagation direction of the incident X-rays. A 10 period sine-wave field of 4.5 Oe ($\sim$7.14 $\times$ 10^5 A/cm^2) amplitude and 160 MHz frequency was used to excite vortex gyrations in disk 1 and/or disk 3, where 160 MHz was the eigenfrequency of the sample disks of the given simulation-obtained dimensions.

Conflict of Interest: The authors declare no competing financial interest.

Supporting Information Available: Simulated differential images for vortex gyration excitations compared to those with no excitation, serial differential XMCD images, simulation results for the concept of OR gate. This material is available free of charge *via* the Internet at http://pubs.acs.org.

REFERENCES AND NOTES

1. Semiconductor Industry Assoc. *International Technology Roadmap for Semiconductors*, 2009 edition; http://public.itrs.net; 2009.
2. Keyes, R. Physical Limits in Semiconductor Electronics. *Science* **1977**, *195*, 1230–1235.
3. Cowburn, R. P.; Welland, M. E. Room Temperature Magnetic Quantum Cellular Automata. *Science* **2000**, *287*, 1466–1468.
4. Imre, A.; Csaba, G.; Ji, L.; Orlov, A.; Bernstein, G. H.; Porod, W. Majority Logic Gate for Magnetic Quantum-Dot Cellular Automata. *Science* **2006**, *311*, 205–208.
5. Csaba, G.; Imre, A.; Bernstein, G. H.; Porod, W. Nanocomputing by Field-Coupled Nanomagnets. *IEEE Trans. Nanotechnol.* **2002**, *1*, 209–213.
6. Imre, A.; Zhou L.; Orlov A.; Csaba G.; Bernstein, G. H.; Porod W.; Metlushko, V. Application of Mesoscopic Magnetic Rings for Logic Devices. 4th IEEE Conference on Nanotechnology, Los Alamitos, CA, Aug **2004**; pp 137−139.
7. Bowden, S. R.; Gibson, U. J. Optical Characterization of All-Magnetic NOT Gate Operation in Vortex Rings. *IEEE Trans. Magn.* **2009**, *45*, 5326–5332.
8. Bowden, S. R.; Gibson, U. J. Logic Operations and Data Storage Using Vortex Magnetization States in Mesoscopic Permalloy Rings, and Optical Readout. *J. Phys.: Conf. Ser.* **2010**, *200*, 072033.
9. Barman, S.; Barman, A.; Otani, Y. Dynamics of 1-D Chains of Magnetic Vortices in Response to Local and Global Excitations. *IEEE Trans. Magn.* **2010**, *46*, 1342–1345.
10. Jung, H.; Yu, Y.-S.; Lee, K.-S.; Im, M.-Y.; Fischer, P.; Bocklage, L.; Vogel, A.; Bolte, M.; Meier, G.; Kim, S.-K. Observation of Coupled Vortex Gyrations by 70-ps-Time- and 20-nm-Space-Resolved Full-Field Magnetic Transmission Soft X-ray Microscopy. *Appl. Phys. Lett.* **2010**, *97*, 222502.
11. Jung, H.; Lee, K.-S.; Jeong, D.-E.; Choi, Y.-S.; Yu, Y.-S.; Han, D.-S.; Vogel, A.; Bocklage, L.; Meier, G.; Im, M.-Y.; *et al.* Tunable Negligible-Loss Energy Transfer between Dipolar-Coupled Magnetic Disks by Stimulated Vortex Gyration. *Sci. Rep.* **2011**, *1*, 59.
12. Vogel, A.; Kamionka, T.; Martens, M.; Drews, A.; Chou, K.; Tyliszczak, T.; Stoll, H.; Van Waeyenberge, B.; Meier, G. Coupled Vortex Oscillations in Spatially Separated Permalloy Squares. *Phys. Rev. Lett.* **2011**, *106*, 137201.
13. Sugimoto, S.; Fukuma, Y.; Kasai, S.; Kimura, T.; Barman, A.; Otani, Y. C. Dynamics of Coupled Vortices in a Pair of Ferromagnetic Disks. *Phys. Rev. Lett.* **2011**, *106*, 197203.
14. Vogel, A.; Martens, M.; Weigand, M.; Meier, G. Signal Transfer in a Chain of Stray-Field Coupled Ferromagnetic Squares. *Appl. Phys. Lett.* **2011**, *99*, 042506.
15. Guslienko, K. Y.; Ivanov, B. A.; Novosad, V.; Otani, Y.; Shima, H.; Fukamichi, K. Eigenfrequencies of Vortex State Excitations in Magnetic Submicron-Size Disks. *J. Appl. Phys.* **2002**, *91*, 8037–8039.
16. Kasai, S.; Nakatani, Y.; Kobayashi, K.; Kohno, H.; Ono, T. Current-Driven Resonant Excitation of Magnetic Vortices. *Phys. Rev. Lett.* **2006**, *97*, 107204.
17. Lee, K.-S.; Guslienko, K. Y.; Lee, J.-Y.; Kim, S.-K. Ultrafast Vortex-Core Reversal Dynamics in Ferromagnetic Nanodots. *Phys. Rev. B* **2007**, *76*, 174410.
18. Kim, S.-K.; Lee, K.-S.; Yu, Y.-S.; Choi, Y.-S. Reliable Low-Power Control of Ultrafast Vortex-Core Switching with the Selectivity in an Array of Vortex States by In-Plane Circular-Rotational Magnetic Fields and Spin-Polarized Currents. *Appl. Phys. Lett.* **2008**, *92*, 022509.
19. Van Waeyenberge, B.; Puzic, A; Stoll, H.; Chou, K. W.; Tyliszczak, T.; Hertel, R.; Fähnle, M.; Brückl, H.; Rott, K.; Reiss, G.; *et al.* Magnetic Vortex Core Reversal by Excitation with Short Bursts of an Alternating Field. *Nature* **2006**, *444*, 461–464.
20. Thornton, S. T.; Marion, J. B. *Classical Dynamics of Particles and Systems*, 5th ed.; Brooks/Cole-Thomson Learning: Belmont, CA; 2004.
21. Lee, K.-S.; Kim, S.-K. Two Circular-Rotational Eigenmodes and Their Giant Resonance Asymmetry in Vortex Gyrotropic Motions in Soft Magnetic Nanodots. *Phys. Rev. B* **2008**, *78*, 014405.
22. Curcic, M.; Van Waeyenberge, B.; Vansteenkiste, A.; Weigand, M.; Sackmann, V.; Stoll, H.; Fähnle, M.; Tyliszczak, T.; Woltersdorf, G.; Back, C. H.; *et al.* Polarization Selective Magnetic Vortex Dynamics and Core Reversal in Rotating Magnetic Fields. *Phys. Rev. Lett.* **2008**, *101*, 197204.
23. Fischer, P. Soft X-ray Microscopy—A Powerful Analytical Tool To Image Magnetism Down to Fundamental Length and Time Scales. *AAPPS Bull.* **2008**, *18*, 12–17.
24. Fischer, P.; Im, M.-Y.; Kasai, S.; Yamada, K.; Ono, T.; Thiaville, A. X-ray Imaging of Magnetic Vortices in Confined Magnetic Structures. *Phys. Rev. B* **2011**, *83*, 212402.
25. Chou, K. W.; Puzic, A.; Stoll, H.; Schütz, G.; Van Waeyenberge, B.; Tyliszczak, T.; Rott, K.; Reiss, G.; Brückl, H.; Neudecker, I.; *et al.* Vortex Dynamics in Coupled Ferromagnetic Multilayer Structures. *J. Appl. Phys.* **2006**, *99*, 08F305.
26. Lee, K.-S.; Kim, S.-K.; Yu, Y.-S.; Choi, Y.-S.; Guslienko, K.; Jung, H.; Fischer, P. Universal Criterion and Phase Diagram for Switching a Magnetic Vortex Core in Soft Magnetic Nanodots. *Phys. Rev. Lett.* **2008**, *101*, 267206.
27. Lee, K.-S.; Jung, H.; Han, D.-S.; Kim, S.-K. Normal Modes of Coupled Vortex Gyration in Two Spatially Separated Magnetic Nanodisks. *J. Appl. Phys.* **2011**, *110*, 113903.
28. Nakano, K.; Chiba, D.; Sekiguchi, K.; Kasai, S.; Ohshima, N.; Kobayashi, K.; Ono, T. Electrical Detection of Vortex Core Polarity in Ferromagnetic Disk. *Appl. Phys. Express* **2010**, *3*, 053001.
29. Nakano, K.; Chiba, D.; Ohshima, N.; Kasai, S.; Sato, T.; Nakatani, Y.; Sekiguchi, K.; Kobayashi, K.; Ono, T. All-Electrical Operation of Magnetic Vortex Core Memory Cell. *Appl. Phys. Lett.* **2011**, *99*, 262505.
30. Ohe, J.; Barnes, S. E.; Lee, H.-W.; Maekawa, S. Electrical Measurements of the Polarization in a Moving Magnetic Vortex. *Appl. Phys. Lett.* **2009**, *95*, 123110.
31. Donahue, M.; Porter, D. *OOMMF User's Guide*, version 1.0, Interagency Report NISTIR 6376; National Institute of Standards and Technology, 1999.